Early aggregation in the soot formation region of an ethylene flame

C. Russo, B. Apicella, A. Tregrossi, M. M. Oliano, A. Ciajolo

Istituto di Ricerche sulla Combustione - C.N.R., Napoli - Italy

Introduction

Fuel oxidation and/or decomposition, polycyclic aromatic hydrocarbon (PAH) formation, particle inception, coagulation, surface growth, aggregation and oxidation, concur all together to soot inception, formation and growth. Specifically, the current view of soot formation starts with particle nucleation, followed by mass and size growth through coalescence, coagulation, surface reactions, and finally by aggregation into fractal structures [1]. That soot particle aggregation is a phenomenon not separated in time from particle nucleation has been suggested [1] and then experimentally observed both in diffusion and laminar premixed flames [2-4]. To get insights on this issue, the present work reports in deep detail the characteristics of carbon particulate produced at the inception in a heavily sooting laminar premixed ethylene flame (equivalence ratio=2.4). The cold gas velocity and the temperature of the flame were chosen enough low to slower soot particle formation kinetics and thereby to widen the inception phase.

Experimental

Sampling

The carbon particulate, produced in an ethylene-oxygen premixed laminar atmospheric flame (C/O= 0.8, cold gas velocity 3cm/s) burning on a water-cooled sintered bronze McKenna burner (d=60mm) (Holthuis & Associates), was deposited on fused silica plates at three height above the burner (HAB), namely 5, 6, 7 mm, near the inception, that occurs at 5 mm. The set-up for the deposition into the flame was composed of a fused-silica plate driven by a gear motor, which regulates the insertion/deposition time of the plate to 60ms per lap. The total deposition time for each sample was set to 25 s.

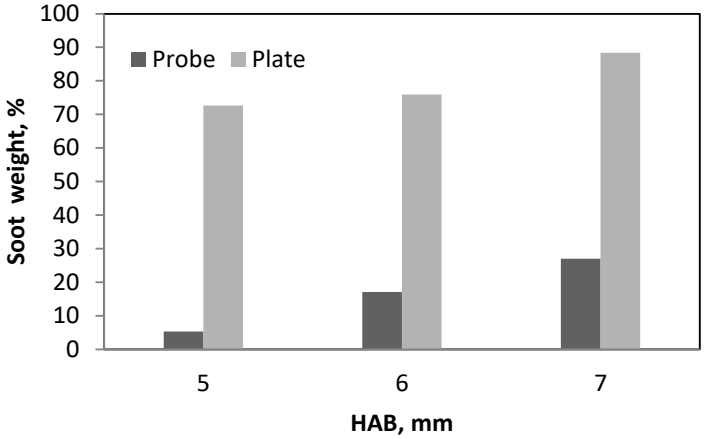

Fig.1 Weight percentage of soot fraction of the total carbon particulate probed and deposited along the ethylene flame.

The organic compounds condensed on the deposited carbonaceous species were separated from the solid carbonaceous species (dry soot) by solubilization in dichloromethane (DCM). This

Corresponding author: Dr. Carmela Russo, carmela.russo@irc.cnr.it

sampling method was faster in comparison to the isokinetic probe, that required longer sampling times for recovering measurable amounts of soot especially in the first phase of soot formation. A comparison between the two sampling methods is reported in Fig.1, where the percentages of DCM-insoluble (soot) fraction along the flame are reported for the ethylene flame. Plate deposition enhances the soot contribution to the total particulate, thus thermophoresis efficiency is higher for soot rather than for condensed phases, allowing the employment of this sampling mode for soot analysis.

Characterization

Raman spectra were measured directly on the soot deposited on quartz plates by means of a Horiba XploRA Raman microscope system (Horiba Jobin Yvon, Japan) with an excitation wavelength of 532 nm. Dry soot was removed from the quartz plates by N-methyl-pyrrolidinone (NMP) treatment in ultrasonic bath and recovered for UV-Visible spectroscopy analysis performed on a HP 8453 spectrometer in the wavelength range of 260-1100nm.
The SEC analysis of soot suspensions in NMP was carried out on a HPLC system HP1050 series by elution with NMP on a Jordi Gel DVB Solid Bead column 300x7.8mm for the molecular weight (MW) determination in the 1E5-1E11u range. The online detection of species eluted from the SEC column used a HP1050 UV-Visible diode array detector that measured the absorbance signal at a fixed absorption wavelength (350 nm). The SEC calibration curve used for the MW evaluation was obtained using polystyrene standards and carbonaceous particles whose MW has been evaluated from the particle diameter measured by Dynamic Light Scattering considering a spherical shape and a density of 1.8 g/cm^3 [5].

Results

UV-Visible and Raman features of soot collected by deposition on a quartz plate and sampled with the isokinetic probe have been compared to verify the sampling mode did not alter the material. The normalized UV-Visible and Raman spectra collected by means of deposition and isokinetic probe at 6 mm HAB are compared in Fig. 2.

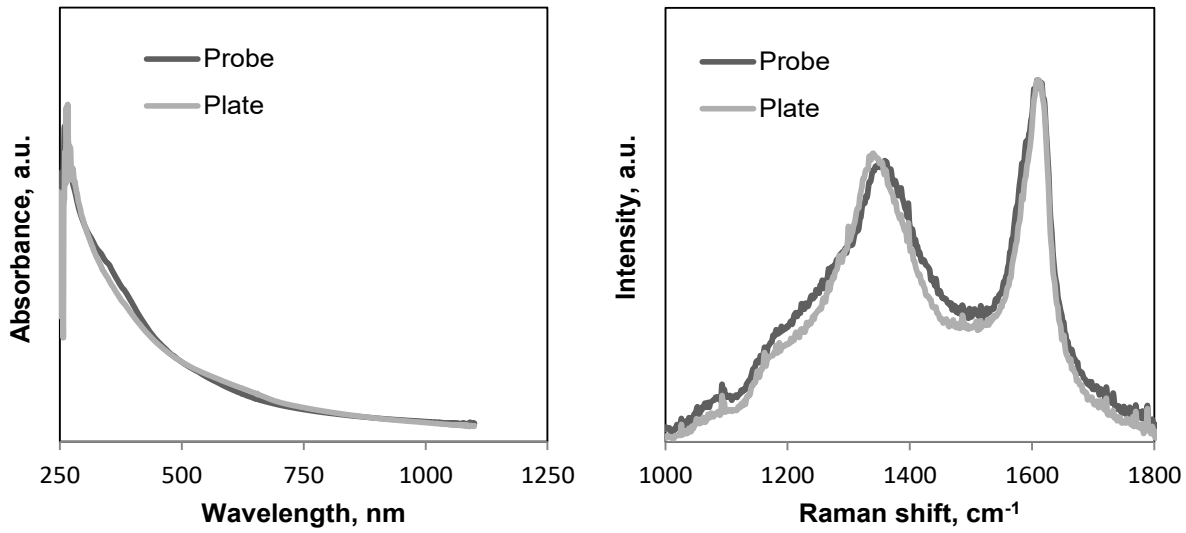

Fig.2 UV-Visible (left part) and Raman (right part) spectra of soot collected by means fused-silica plate deposition and isokinetic probe at 6 mm HAB.

The Raman spectra were continuum subtracted with a linear correction between 1000 and 1800 cm^{-1}. The two typical peaks of carbon materials, near 1600 cm^{-1} (G or "graphite" peak) and 1350 cm^{-1} (D or "defect" peak), can be observed in the first order spectral Raman region, between 1000-1800 cm^{-1} [6]. The peaks broadness underlies the highly disordered structures of soot. Beside the D and G bands, other minor modulations, induced by defects outside and

inside the crystal lattice, occur. Comparing the UV-Visible spectra, it can be seen that while visible features (absorption for wavelength higher than 500nm) are comparable, soot collected with the isokinetic probe presents in the UV region a fine spectral structure typical of condensed species. The presence of this amorphous-like material could be also responsible for the higher broadness of the D peak of the Raman spectrum in comparison with that featuring soot deposited with the quartz plate. Thus, it is confirmed that quartz deposition mode allowed a proper comparison of soot particles/aggregates, presenting a lower efficiency collection for lower molecular weight compounds.

MW distribution of flame-formed soot obtained by SEC analysis, reported in Fig. 3 show the typical multimodality extended throughout a wide MW range (200–1E11 u). The relative increase of the higher MW peak intensity can be noticed as the HAB increases from 5 to 7 mm. The peak 3 is attributed to residual condensed species not removed with DCM-extraction, the peak 2 is due to single particles and the peak 1 to particle aggregates [5].

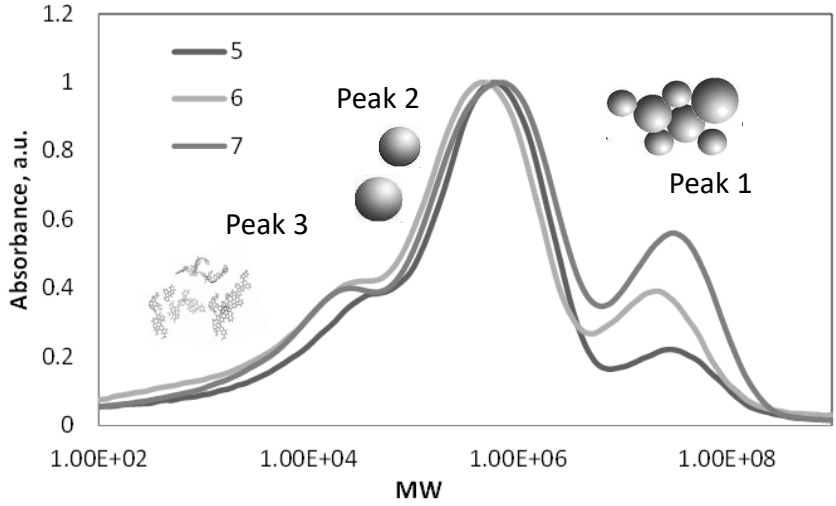

Fig. 3 MW distribution obtained by SEC of soot collected by means fused-silica plate deposition at different HAB.

The peak related to soot aggregates is always present and its relative intensity increases as the HAB increases, testifying an increasing relevance of the aggregation phenomenon that occurs since the beginning of soot formation.

The energy band gap was evaluated by using the Tauc relation: $(A \times E)^{0.5} = B \times (E - Eg)$ [7], where A is the absorbance, E is the energy of the incident photon, B is a constant and Eg is the optical band gap evaluated on the visible tail of the Tauc spectra by extrapolation to zero absorption. The optical band gap values, Eg, reported in Table 1 were evaluated on the on-line spectra collected on the apex of the SEC peaks representative of the main MW-segregated fractions. In Table 1 the band gap values evaluated on the UV-Visible spectrum of the bulk soot suspension are also reported.

It can be seen the band gap value evaluated on the bulk is very close to that evaluated on the on-line spectrum measured for the aggregate peak (peak 1), showing that the optical/electronic properties of soot are nearer to that of the soot aggregates (peak 1) already present in the inception flame region.

Table 1 Band gap of soot evaluated on the on-line UV-Visible spectra of the main MW-segregated fractions measured by SEC and on the UV-Visible spectrum of the bulk NMP suspension.

HAB, mm	***Eg, eV***		
	Bulk	***MW fraction***	
5	0.9	peak 1	0.76
		peak 2	1.33
		peak 3	1.6
6	0.95	peak 1	0.6
		peak 2	1.3
		peak 3	1.64
7	0.9	peak 1	0.72
		peak 2	1.22
		peak 3	1.52

It can be concluded that low optical band gap of soot are mainly determined by, even few, soot aggregates, and at the same time such optical band gaps testify the simultaneous occurrence of soot inception and aggregation. Further work is in course to verify this finding and the implications on soot inception mechanism.

References

[1] Frenklach, M. Reaction mechanism of soot formation in flames, Phys. Chem. Chem. Phys. 4 (2002) 2028-2037.
[2] Di Stasio S. Electron microscopy evidence of aggregation under three different size scales for soot nanoparticles in flame. Carbon 2001; 39:109-118.
[3] Kholghy M, Saffaripour M, Yip C, Thomson MJ. The Evolution of Soot Morphology in an Atmospheric Laminar Coflow Diffusion Flame of a Surrogate for Jet A-1. Comb. Flame 2013; 160:2119-2130.
[4] Russo C., Apicella B., Lightly J. S., Ciajolo A, Tregrossi A. Optical properties of organic carbon and soot produced in an inverse diffusion flame. Carbon 2017; 124: 372-379.
[5] D'Anna A, Ciajolo A, Alfè M, Apicella B, Tregrossi A. Effect of fuel/air ratio and aromaticity on the molecular weight distribution of soot in premixed n-heptane flames. Proc. Combust. Inst. 2009; 32:803-810.
[6] Tauc J, Grigorovici R, Vancu A. Optical Properties and Electronic Structure of Amorphous Germanium. Phys. Status Solidi B 1966; 15:627-637.
[7] Ferrari AC, Robertson J. Interpretation of Raman spectra of disordered and amorphous carbon. Physical Review B 2000; 61:14095-14107.